Acta Crystallographica Section A
Foundations of Crystallography
ISSN 0108-7673

Received 31 January 2004
Accepted 15 July 2004

Topological properties of the electron density of solids and molecules. Recent developments in Oviedo

Víctor Luaña,[a]* Aurora Costales,[a] Paula Mori-Sánchez,[a,b] Miguel A. Blanco[a] and A. Martín Pendás[a]

[a]Departamento de Química Física y Analítica, Universidad de Oviedo, E-33006 Oviedo, Spain, and [b]Department of Chemistry, Duke University, Box 90354, Durham, NC 27708-0354, USA. Correspondence e-mail: victor@carbono.quimica.uniovi.es

Some of the latest advances in the analysis of electron density are reviewed, including: (*a*) topological indices that provide a useful characterization of the global properties of the density; (*b*) specific results on some prototypical metal and low heteropolarity systems; and (*c*) calculation of the local curvature of the interatomic surface.

1. Introduction

Thoroughly grounded on fundamental quantum principles, the atoms-in-molecules theory, AIM (Bader, 1990), provides a useful and practical tool for the analysis and classification of molecules and crystals based on their bonding properties. We describe in this report four different new applications of the theory that have been recently developed within our research group.

2. Topological indices

Compounds are routinely classified into the broad categories of ionic, covalent and metallic by using different empirical criteria. Perhaps the best known classification is the van Arkel–Ketelaar diagram (van Arkel, 1956; Ketelaar, 1958), based on the electronegativity difference and the electronegativity average of the elements. A similar scheme can be based on bond electron-density properties (Mori-Sánchez *et al.*, 2002). The main separation is provided by two indices:

(i) a *charge transfer* index, $c = \langle Q_\Omega / \mathrm{OS}_\Omega \rangle$, defined as the average for all basins of the ratio between the actual topological charge and the expected oxidation state; and

(ii) a *flatness* index, f, defined as the ratio between the absolute minimum of the electron density in the crystal and the highest electron density on a bond critical point (CP).

Most crystals made of a single element have $\mathrm{OS}_\Omega = Q_\Omega = 0$ and are assigned $c = 0$ as a default. On the other hand, many molecular crystals are revealed by the *molecularity* index, μ, defined as the relative difference between the highest and the lowest bond CP's if their Laplacians have different sign.

The diagram in Fig. 1 shows that the charge-transfer index provides a clear separation between ionic and covalent crystals. Large electron-density flatness values are specific of metals and metallic alloys. Large values of the μ index are found in N_2, N_2O_3 and graphite crystals, for instance.

3. Electron density of alkali metals

From the large collection of compounds contained in Fig. 1, let us give particular attention to the alkali metals. There has recently been some discussion on the actual topology of these crystals, particularly on the occurrence or not of *non-nuclear maxima* (NNM) of the electron density (Sakata & Sato, 1990; Iversen *et al.*, 1995; de Vries *et al.*, 1996; Iversen *et al.*, 1997; Jayatilaka, 1998; Martín Pendás *et al.*, 1999; Madsen *et al.*,

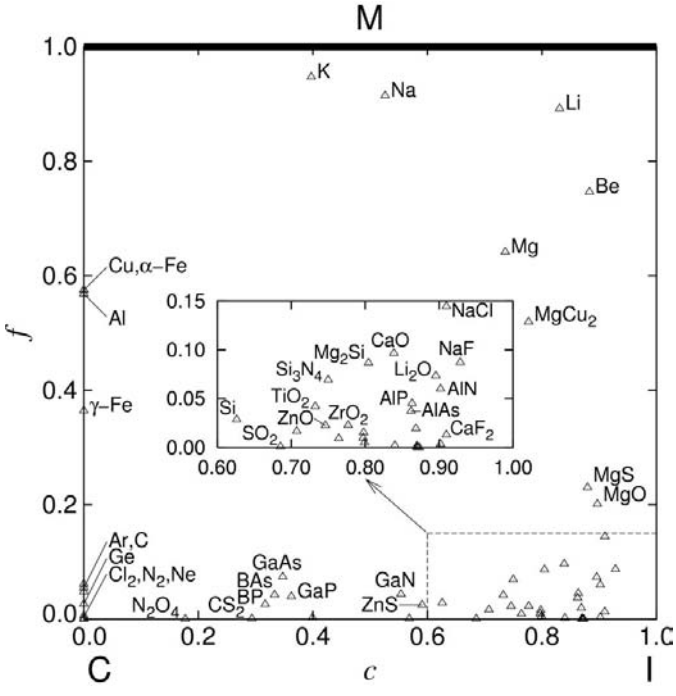

Figure 1
Topological classification of crystals according to the charge transfer and flatness indices. This diagram is based on HF/LCAO calculations (Pisani & Dovesi, 1980) at the experimental geometries.

2002). Therefore, we have tried and compared several theoretical methods for obtaining the electron density (Luaña *et al.*, 2003), even though we will only examine here our best fpLAPW/GGA results, obtained using Blaha and Schwarz's *WIEN* code (Blaha *et al.*, 1990, 1999).

With a flatness of nearly one, alkali metals are close to a uniform gas model. Two significant consequences of this are a tendency to form non-nuclear maxima and a tendency towards easy topological change. Both features are spectacularly apparent in the case of b.c.c. lithium. According to our fpLAPW/GGA calculations, NNM fill about 76% of the crystal volume at the experimental geometry, and contain some 0.8 e donated from each Li atom. In a sense, this topological image of lithium corresponds to an ionic crystal where the spherical Li^+ cores are the convex cations and the NNM play the role of the anions. In a different way, this lithium density can be presented like an almost ideal Drude metal made of a nearly flat valence-electron sea anchored to a periodic network of Li^+ cores.

This topology is, however, not stable and small changes in the crystal volume, representing the application of hydrostatic pressure, give rise to large changes in the topology. We have found 20 different topologies for b.c.c. Li when the lattice parameter varies in the range 4–9 bohr. Our main results for lithium are recalled in Fig. 2. We can see, represented against the lattice parameter, the total energy (left scale) and the valence-electron-density flatness (right scale) plus, represented on the horizontal scales, the sequence of all topologies.

Fortunately, the very many topologies found for all the alkali metals can be organized into just five different significant types. For long distances, usually larger than the equilibrium values, there exists a B_2 topology where first and second neighbors are bonded. At smaller distances, we find a B_1 topology where only first neighbors remain bonded. At even smaller distances, we can find up to three different topologies showing NNM: either twin or single NNM along the metal–metal line or interstitial NNM (M_g, M_L and M_i, respectively).

Fig. 3 shows that the five alkali metals follow the same sequence of topologies upon compression: B_2, B_1, eventually NNM and again B_2 as the inner electronic shells start to interact. We can see that lithium shows NNM over a wide range of geometries, including the equilibrium distance R_e at zero pressure. Na, on the other hand, needs a small compression before NNM can be found, and the range of their existence is much smaller than in the case of Li. The behavior of potassium is similar to that of sodium. Again it is necessary to compress slightly the crystal before NNM appear, and the NNM range is now rather short. Finally, neither rubidium nor caesium present NNM, even if we apply a very large compression.

The examination of the actual charge carried out by the NNM completes the big picture. Whereas the Li atoms give away up to 0.8 e to the lattice, the Na atoms donate 0.3 e at most and the K atoms less than 0.1 e. It is easy to conclude that NNM are mostly a phenomenon of light atoms. As a final aside, it is quite significant that all the above results can be explained by considering the promolecular or Hartree–Fock (HF) electron densities of diatomic M_2 or tetrahedral-like M_4 clusters (Luaña *et al.*, 2003).

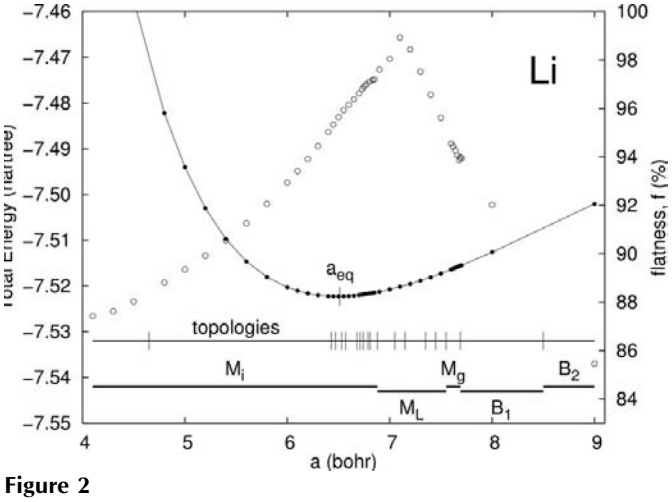

Figure 2
Summary of the fpLAPW/GGA calculations on b.c.c. lithium. The properties represented are: total energy (solid line and black dots), electron-density flatness (empty circles), range of existence of each detailed topology and of each topological regime (see text for the definition of B_1, B_2, M_g *etc.*).

4. Low heteropolarity compounds

The large variability of the electron-density topology shown in the previous figures is quite characteristic of simple metals and metallic alloys. Usually, ionic and covalent crystals have a single topology, which is mainly determined by the crystal geometry and some atomic size ratios (Luaña *et al.*, 1997; Martín Pendás *et al.*, 1998). We have found, however, that boron phosphide presents a peculiar and rare behavior (Mori-Sánchez *et al.*, 2001). Under ambient pressure, boron behaves as a small cation carrying a charge of about +1 e. Upon compression, a small NNM is formed before the polarity is

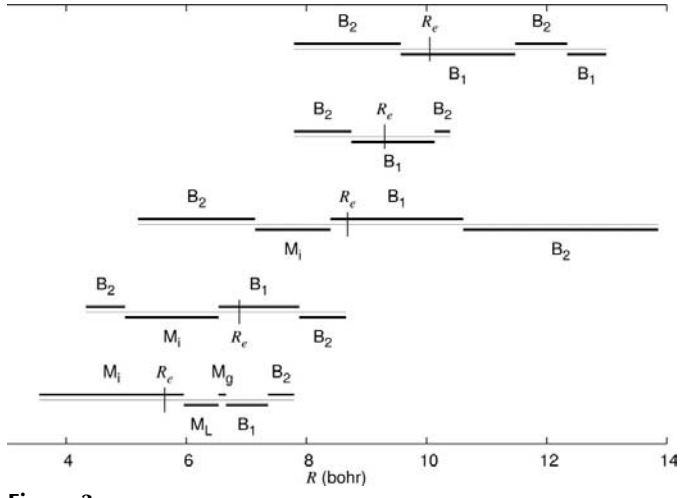

Figure 3
Main topological changes shown by all b.c.c. alkali metals. From bottom to top: Li, Na, K, Rb, Cs.

Table 1
Topological properties at the O—H BCP in H_2O; all values are in atomic units, except R_{OH} in Å and $\alpha = \alpha_{HOH}$ in °.

Calculation	R_{OH}	α	ρ_b	$\nabla^2\rho_b$	K	κ_b
HF/3-21G	0.9667	107.7	0.33071	−1.4439	0.45854	0.0102
HF/6-31G	0.9496	111.5	0.35359	−1.7247	0.97793	0.0286
HF/6-31G(d,p)	0.9431	106.0	0.39106	−2.4431	1.67982	0.0442
HF/6-311G(3df,p)	0.9408	105.6	0.39002	−2.9225	1.46507	0.0528
B3LYP/6-311G(3df,p)	0.9618	104.0	0.36745	−2.5299	0.80936	0.0503
MP2/6-311G(3df,p)	0.9505	103.5	0.36316	−2.5461	1.03112	0.0565
CISD/6-311G(3df,p)	0.9408	105.6	0.37238	−2.6314	1.03120	0.0545

finally reversed, boron becomes the anion rather than the cation and, therefore, boron phosphide becomes phosphorus boride. The plot of the electron-density Laplacian, together with the interatomic surfaces and bond paths, see Fig. 4, reveals that the polarity inversion occurs not because of a severe reorganization of the crystal electron density but, rather, because the interatomic surface is displaced from the neighborhood of B to the neighborhood of P. The transformation, on the other hand, appears to be related in this crystal to the emergence of a metallic phase. This very special behavior of the BP crystal is actually related to the quite similar electronegativities of both atoms. Similar interesting phenomena can be expected from other low-heteropolarity compounds.

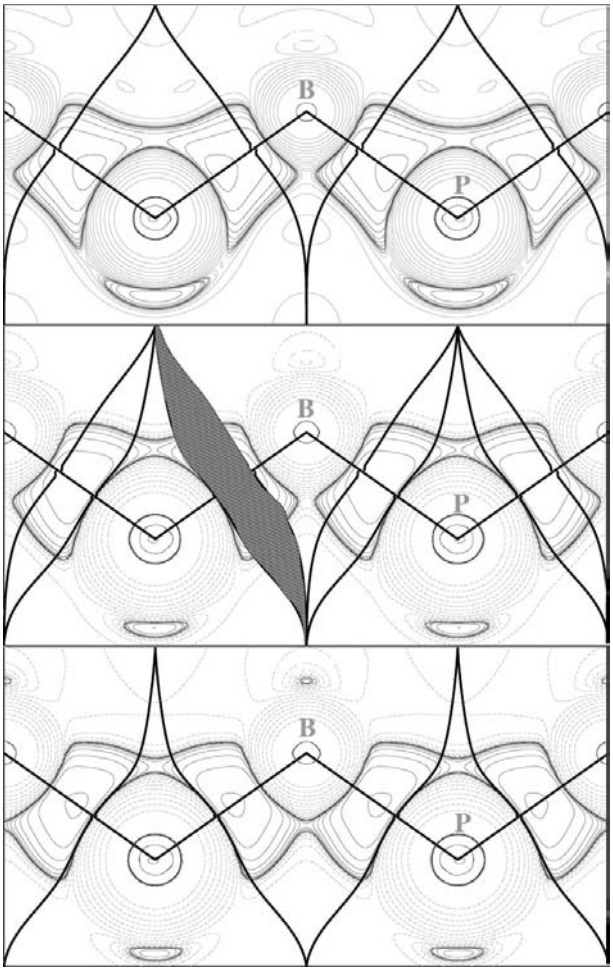

Figure 4
[110] plane of the BP crystal, containing three B and two P nuclei. The plots correspond to lattice parameters of 4.55 (top), 3.93 (middle) and 3.75 Å (bottom). Thick solid lines show the bond paths and the atom basin boundaries. The contour lines depict the electron-density Laplacian $[\nabla^2\rho(\mathbf{r})]$. One of the NNM basins is shown as a darkened area in the middle map.

5. Curvature of the interatomic surfaces

Topological analysis is based on the capability to determine first and second derivatives of the electron density at any point. By being able to determine also the third derivatives, we can access the curvatures of gradient lines and interatomic surfaces (IAS). The curvature of a given IAS near the bond critical point is one of its most easily noticeable geometrical features. However, the lack of local descriptions for separation surfaces in dynamical systems has made difficult any investigation about its origin. The analytical expressions that we have published recently (Martín Pendás & Luaña, 2003*a*,*b*) change this scenario, for now it becomes possible to examine the curvatures at bond critical points (BCP), for instance, in terms of local derivatives of ρ.

Let us briefly recall the main concepts involved. All the expressions that follow are referred to the principal reference frame at the critical point (Martín Pendás & Luaña, 2003*a*). This is the frame formed by the eigenvectors of the Hessian of ρ at the BCP, in such a way that the z axis corresponds to the bond-path direction (eigenvector of the positive Hessian eigenvalue at the BCP), and the x, y axes along the orthogonal eigenvectors chosen so as to form a right-handed frame. Let us define the coefficients

$$A_{\alpha\beta\gamma} = \frac{\rho_{\alpha\beta\gamma}}{\rho_{\alpha\alpha} + \rho_{\beta\beta} - \rho_{\gamma\gamma}}, \tag{1}$$

where ρ_α, $\rho_{\alpha\beta}$ and $\rho_{\alpha\beta\gamma}$ are first, second and third derivatives of the density at the BCP calculated in the principal frame. It follows, then, that the principal normal vectors of the gradient lines along the x, y, z directions at the critical point are

$$\begin{aligned}(\kappa\mathbf{n})^x &= A_{xxy}\mathbf{j} + A_{xxz}\mathbf{k},\\ (\kappa\mathbf{n})^y &= A_{yyx}\mathbf{i} + A_{yyz}\mathbf{k},\\ (\kappa\mathbf{n})^z &= A_{zzx}\mathbf{i} + A_{zzy}\mathbf{j},\end{aligned} \tag{2}$$

where κ is the curvature of the specified gradient line and $\mathbf{n}$ its unit principal normal vector. Moreover, the Gaussian curvature at the BCP is

Table 2
Topological properties at the *A*–H BCP in the hydrogen saturated molecules of the first period according to HF/TZV++(3df,2p) calculations at the theoretical equilibrium distance *R*; all values in atomic units.

System	*R*	Shape	*K*	$\nabla^2\rho_b$	ρ_b	Q_H
LiH	3.0303	*A*(H	0.1005	+0.1420	0.0390	−0.9040
BeH_2	2.5152	*A*(H	0.2427	+0.2225	0.0971	−0.8511
BH_3	2.2434	*A*(H	0.1780	−0.3180	0.1862	−0.6960
CH_3	2.0446	*A*)H	0.1019	−1.0436	0.2837	−0.0354
NH_3	1.8868	*A*)H	0.3510	−1.9089	0.3552	+0.3550
OH_2	1.7766	*A*)H	1.5433	−3.0992	0.3883	+0.6322
FH	1.6956	*A*)H	3.5514	−3.8718	0.3945	+0.7765

$$K = A_{xxz}A_{yyz} - A_{xyz}^2. \quad (3)$$

Table 1 shows the convergence of O—H BCP properties in H_2O, calculated with several basis sets and several theoretical methods. The convergence of the Gaussian curvature of the O)H IAS, *K*, is more difficult than that of the bond density, ρ_b, but similar to the convergence of the bond Laplacian, $\nabla^2\rho_b$. Adding flexibility to the basis set, particularly including polarization functions, increases the curvature significantly. On the contrary, the correlation effects tend to lower the curvature and smooth out the IAS. The O—H bond-path curvature, κ_b, is rather small, as it corresponds to an unstressed bonding line.

Table 2 collects the topological properties at the *A*—H BCP for the hydrogen-saturated molecules of the second period. Firstly, we observe that the compounds usually called hydrides, LiH, BeH_2 and BH_3, display IAS curving towards the non-H atom, *A*(H, with topological charges consistent with their nominal oxidation states. On the contrary, H acts as a cation for NH_3, H_2O and HF and the IAS curves accordingly towards the H cation: *A*)H. CH_3 is an interesting system as it marks the sign change for the curvatures in the series and it provides an example where the charge-transfer curvature correlation, sometimes assumed, is violated.

Bond distance and charge transfer can be shown to influence the IAS Gaussian curvature. In going from CH_3 to HF, the shortening in the bond distance and the increasing charge transfer contribute together to increase *K*, up to the point that the Gaussian curvature of HF is the highest that we have found in our explorations so far.

We thank the Spanish Ministerio de Ciencia y Tecnología for financial support under projects BQU2000-0466 and BQU2003-06553. PMS is currently a Fulbright fellow. ACC is a Ramón y Cajal fellow.

References

Arkel, A. E. van (1956). In *Molecules and Crystals in Inorganic Chemistry*. New York: Interscience.
Bader, R. F. W. (1990). *Atoms in Molecules. A Quantum Theory*. New York: Oxford University Press.
Blaha, P., Schwarz, K. & Luitz, J. (1999). *WIEN97, a Full Potential Linearized Augmented Plane Wave Package for Calculating Crystal Properties*, K. Schwarz, Technical University Wien, Vienna, ISBN 3-9501031-0-4.
Blaha, P., Schwarz, K., Sorantin, P. & Trickey, S. B. (1990). *Comput. Phys. Commun.* **59**, 399,.
Iversen, B. B., Jensen, J. L. & Danielsen, J. (1997). *Acta Cryst.* A**53**, 376–387.
Iversen, B. B., Larsen, F. K., Souhassou, M. & Takata, M. (1995). *Acta Cryst.* B**51**, 580–591.
Jayatilaka, D. (1998). *Phys. Rev. Lett.* **80**, 798–801.
Ketelaar, J. A. A. (1958). *Chemical Constitution: an Introduction to the Theory of the Chemical Bond*, 2nd ed. New York: Elsevier.
Luaña, V., Costales, A. & Martín Pendás, A. (1997). *Phys. Rev. B*, **55**, 4285–4297.
Luaña, V., Mori-Sánchez, P., Costales, A., Blanco, M. A. & Martín Pendás, A. (2003). *J. Chem. Phys.* **119**, 6341–6350.
Madsen, G. K. H., Blaha, P. & Schwarz, K. (2002). *J. Chem. Phys.* **117**, 8030–8035.
Martín Pendás, A., Blanco, M. A., Costales, A., Mori-Sánchez, P. & Luaña, V. (1999). *Phys. Rev. Lett.* **83**, 1930–1933.
Martín Pendás, A., Costales, A. & Luaña, V. (1998). *J. Phys. Chem. B*, **102**, 6937–6948.
Martín Pendás, A. & Luaña, V. (2003*a*). *J. Chem. Phys.* **119**, 7643–7650.
Martín Pendás, A. & Luaña, V. (2003*b*). *J. Chem. Phys.* **119**, 7633–7642.
Mori-Sánchez, P., Martín Pendás, A. & Luaña, V. (2001). *Phys. Rev. B*, **63**, 125103–1–4.
Mori-Sánchez, P., Martín Pendás, A. & Luaña, V. (2002). *J. Am. Chem. Soc.* **124**, 14721–14723.
Pisani, C. & Dovesi, R. (1980). *Int. J. Quantum Chem.* **17**, 501–516.
Sakata, M. & Sato, M. (1990). *Acta Cryst.* A**46**, 263–270.
Vries, R. Y. de, Briels, W. J. & Feil, D. (1996). *Phys. Rev. Lett.* **77**, 1719–1722.